Applied Physics Letters

RESEARCH ARTICLE | MARCH 17 2022

Zero-field routing of spin waves in a multiferroic heterostructure

Weijia Zhu ; Huajun Qin ; Lukáš Flajšman ; Tomoyasu Taniyama ; Sebastiaan van Dijken

Appl. Phys. Lett. 120, 112407 (2022)
https://doi.org/10.1063/5.0086430

AIP Publishing

Applied Physics Letters ARTICLE scitation.org/journal/apl

Zero-field routing of spin waves in a multiferroic heterostructure

Cite as: Appl. Phys. Lett. **120**, 112407 (2022); doi: 10.1063/5.0086430
Submitted: 25 January 2022 · Accepted: 7 March 2022 ·
Published Online: 17 March 2022

Weijia Zhu,[1] Huajun Qin,[1,a)] Lukáš Flajšman,[1] Tomoyasu Taniyama,[2] and Sebastiaan van Dijken[1,a)]

AFFILIATIONS

[1]NanoSpin, Department of Applied Physics, Aalto University School of Science, P.O. Box 15100, FI-00076 Aalto, Finland
[2]Department of Physics, Nagoya University, Furo-cho, Chikusa-ku, Nagoya 464-8602, Japan

[a)]**Authors to whom correspondence should be addressed:** huajun.qin@aalto.fi and sebastiaan.van.dijken@aalto.fi

ABSTRACT

We report zero-field routing of spin waves in a multiferroic heterostructure comprising a ferromagnetic Fe film and a ferroelectric $BaTiO_3$ substrate with fully correlated strain-coupled domains. In the Fe film, a regular alternation of magnetic anisotropy produces a back-and-forth rotation of uniform magnetization in zero magnetic field. Spin waves propagating across this domain structure are refracted at the magnetic domain walls because of abrupt changes in the dispersion relation and phase velocity. Using super-Nyquist sampling magneto-optical Kerr effect microscopy, we image the routing of spin waves and analyze the dependence of the effect on frequency and the propagation direction. We find that spin waves are routed efficiently by angles up to 60° without measurable loss in amplitude. The experimental results are reproduced by micromagnetic simulations and calculations based on the modified Snell's law for magnonics.

Magnonics, using spin waves as information carriers for data processing, transport, and storage, offers perspectives for low-power wave-like computing.[1–6] Low-loss interconnects enabling the redirection of propagating spin waves are crucial for integrated magnonic circuits. Curved waveguides have been considered as the prime candidate to fulfill this function,[7–11] but the steering of spin waves through bends is complicated by scattering and inefficient mode conversion. Being inspired by optics, magnonic elements with a graded refractive index have been proposed for the redirection and focusing of spin waves with low loss.[12–18] In theory, a smooth spatial variation of the refractive index requires a gradual change of the saturation magnetization, magnetic anisotropy, film thickness, or external magnetic field. Experimental proof-of-concepts of graded-index steering effects have been demonstrated using shape anisotropy[12] and laser-induced heating.[19,20] Another means of redirecting spin waves is through an interface refraction effect, which is described by a modified version of Snell's law.[21–26] Refraction in magnonics occurs when the dispersion relation of spin waves changes abruptly. In experiments, the effect has been demonstrated in magnetic films with a thickness step[21,22] or a magnetic domain wall.[26]

In this Letter, we report on spin-wave refraction in a $Fe/BaTiO_3$ multiferroic heterostructure. In our composite material system, strain-coupling between the ferroelectric substrate and ferromagnetic film produces a regular alternation of magnetic anisotropy and the spin-wave dispersion relation. The heterostructure can, therefore, be considered as an experimental demonstration of a refractive-index grating. Using super-Nyquist sampling magneto-optical Kerr effect (SNS-MOKE) microscopy, we image zigzag-like routing of spin waves across multiple domains and gauge its dependence on the spin-wave frequency and the propagation direction. Our results are a step toward the realization of voltage-controllable refractive-index gratings for magnonics.

The $Fe/BaTiO_3$ multiferroic heterostructure consists of fully correlated ferroelectric/ferromagnetic domains, as illustrated in Fig. 1(a). Two strain-coupled domains alternate in the sample with a period of $\sim 30\,\mu$m. Ferroelectric $BaTiO_3$ domains with perpendicular polarization couple to Fe domains with biaxial magnetic anisotropy. The easy axes of magnetization in these domains and the domain walls make an angle of 45°. Hereafter, we refer to them as *c* domains. $BaTiO_3$ domains with in-plane polarization couple to Fe domains with uniaxial magnetic anisotropy. The easy magnetization axis of these so-called *a* domains aligns parallel to the domain walls. Because of the regular alternation of magnetic anisotropy, the magnetic domain walls in the Fe film are pinned onto the ferroelectric boundaries of $BaTiO_3$.[27]

In our experiments, the fully correlated multiferroic domain pattern is formed during molecular beam epitaxy of a 26-nm-thick Fe film onto a $BaTiO_3$ substrate, as described elsewhere.[28,29] Strain coupling of ferroelectric and ferromagnetic domains has been used to

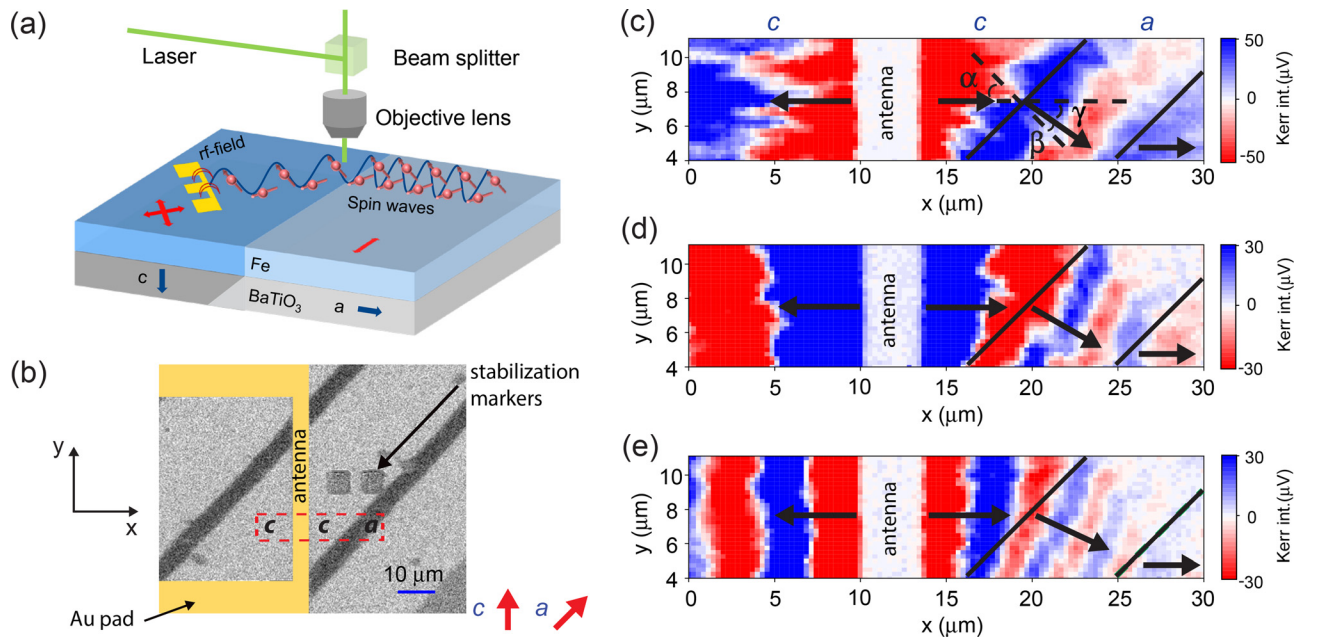

FIG. 1. (a) Schematic of the sample and measurement geometry. Strain coupling between a $BaTiO_3$ substrate and a Fe film produces a fully correlated multiferroic domain structure. In the Fe film, domains with biaxial and uniaxial magnetic anisotropy alternate. Spin waves are excited by a microwave antenna in a *c* domain, and their transport is imaged using SNS-MOKE microscopy in zero magnetic field. (b) MOKE microscopy image of the magnetic domain structure in the Fe film and the position of a microwave antenna patterned on top. The red arrows depict the direction of magnetization in the *a* and *c* domains. The dashed red box indicates the imaging area in SNS-MOKE microscopy measurements. (c)–(e) SNS-MOKE microscopy images of spin-wave transport across a $c-a-c$ domain structure recorded at 9.5 GHz (c), 10.5 GHz (d), and 11.5 GHz (e). The solid lines mark the location of magnetic domain walls. Arrows depict the direction of spin-wave propagation. Transport of spin waves across the magnetic domains is characterized by the incident angle $\alpha = 45^\circ$, the refraction angle β, and the routing angle γ, as illustrated in (c). β and γ depend on the spin-wave frequency.

control magnetic domain-wall motion[29] and spin-wave propagation[30] by an applied electric field. Here, we utilize the multiferroic heterostructure to investigate the redirection of spin waves when they propagate across a $c-a-c$ domain pattern. Spin waves are excited by 3.5-μm-wide microwave antennas with a 3 nm Ta/120 nm Au structure, which are patterned onto the sample using laser-writing lithography and liftoff. A 20-nm-thick insulating TaO_x layer separates the microwave antennas from the Fe film. Spin-wave transport is imaged using SNS-MOKE microscopy. In this technique, the laser frequency comb down-converts the excited GHz magnetization dynamics to an intermediate frequency ε, allowing tuning of the excitation signal to any frequency $f_{exc} = n \times f_{rep} + \varepsilon$. At non-zero ε and with the excitation synchronized to a laser repetition rate of $f_{rep} = 80$ MHz, the phase of the spin waves relative to the excitation signal is preserved by lock-in demodulation at ε.[31] Our home-built SNS-MOKE microscope uses a 515 nm laser with a spot size of ~500 nm. Images are recorded by scanning the Fe/$BaTiO_3$ sample in front of the fixed laser spot with a piezo-controlled stage. In all experiments, the magnetization in the *a* and *c* domains is initialized by applying a magnetic field along the *y* axis. After the magnetic field is turned off, the magnetization aligns at a 45° angle [see red arrows in Fig. 1(b)]. Spin-wave transport is imaged for this configuration in zero magnetic field.

Figures 1(c)–1(e) show SNS-MOKE microscopy images of propagating spin waves at a frequency of 9.5 GHz [Fig. 1(c)], 10.5 GHz [Fig. 1(d)], and 11.5 GHz [Fig. 1(e)]. In the experiments, spin waves are excited within a *c* domain where they propagate perpendicular to the magnetization direction [Damon–Eshbach (DE) transport geometry]. The angle of incidence, α, with respect to the domain wall is therefore 45°. The wavelength shortens and the propagation direction rotates when the spin waves enter the *a* domain. To quantify the redirection of spin waves, we define a refraction angle, β, and a routing angle, $\gamma = \alpha - \beta$. The routing angle is largest just above the FMR frequency of the *c* domain [$\gamma = 41^\circ$ at 9.5 GHz in Fig. 1(c)], and it decreases at higher frequency [$\gamma = 29^\circ$ at 11.5 GHz in Fig. 1(e)]. After transport across the 6-μm-wide *a* domain, the spin waves revert to their original wavelength and propagation direction when entering the second *c* domain. The zigzag-like routing of spin waves that we observe in our multiferroic heterostructure is analogous to the optical beam path in multilayers with alternating refractive indices. In magnonics, a similar effect has been calculated in Refs. 13 and 14. In our experiments, the back-and-forth redirection of spin waves is caused by a regular modulation of magnetic anisotropy induced by strain coupling to ferroelectric domains.

We note that the 45° magnetic domain walls in our multiferroic heterostructure are transparent to propagating spin waves at 9.5–11.5 GHz. Using a different initialization process, the magnetization of neighboring domains can also align at a 135° angle in zero field. In this magnetization configuration, the pinned magnetic domain walls partially reflect the incoming spin waves. Spin-wave reflection is explained by the excitation of a domain-wall resonance, as previously reported for 90° magnetic domain walls in another multiferroic heterostructure.[32]

We performed micromagnetic simulations in MuMax3[33] to analyze the transport of spin waves across the $c-a-c$ domain structure. Figure 2(a) illustrates the simulation geometry. We consider a 26-nm-thick Fe film and an area of $115\times115\,\mu m^2$, discretized into $4\times4\times26\,nm^3$ cells. In the simulations, a 10-μm-wide a domain separates two larger c domains. The uniaxial and biaxial anisotropy values are set to $K_a=15\times10^3$ and $K_c=44\times10^3$ J/m^3, which we experimentally derived from ferromagnetic resonance measurements on single a and c domains.[30] Saturation magnetization $M_s=1705$ kA/m and Gilbert damping parameter $\alpha=0.002$, also extracted from experiments,[30] and exchange constant $A_{ex}=21$ pJ/m[34] are the other input parameters. Spin waves are excited locally by a 1 mT in-plane sinusoidal magnetic field applied over a 400-nm-wide area in the c domain, as indicated by the yellow bar in Fig. 2(a). No magnetic field is applied in the simulations.

Figures 2(b)–2(d) show simulated spatial maps of propagating spin waves at a frequency of 9.5 GHz [Fig. 2(b)], 10.5 GHz [Fig. 2(c)], and 11.5 GHz [Fig. 2(d)]. The simulation results and the SNS-MOKE microscopy measurements shown in Figs. 1(c)–1(e) agree well. From the datasets, we extract the wave vectors of the propagating spin waves in the two magnetic domains as a function of frequency. The results are plotted in Fig. 2(e), together with calculations based on the Kalinikos and Slavin model.[35] The dispersion curve of the c domain at $\alpha=45°$ is shifted up in frequency compared to that of the a domain, which explains the wavelength up and downconversion when spin waves travel from c to a and from a to c, respectively. For the a domain, we calculate the dispersion relation for different refraction angles β, as this parameter changes with frequency. Using the data in Fig. 2(e), we also derive the frequency dependence of the phase velocity in the two magnetic domains for $\alpha=45°$ and $\beta=0°$, i.e., for DE spin waves in the c and a domains [Fig. 2(f)]. Clearly, the difference in phase velocity diminishes at higher frequency.

Transport of spin waves across the magnetic domains of our multiferroic heterostructure is described by a modified version of Snell's law.[21–26] For spin waves traveling from a c domain into an a domain across a pinned magnetic domain wall, Snell's law postulates that the incident angle and wave vector in the c domain and the refraction angle and wave vector in the a domain relate as

$$\frac{\sin\alpha}{\sin\beta}=\frac{k_{refr}}{k_{in}}. \tag{1}$$

The wave vectors in this expression can be calculated using the spin-wave dispersion relation, which is given by Ref. 35,

$$f=\sqrt{\left(\omega_H+\frac{2A\omega_M k^2}{\mu_0 M_s^2}\right)\left(\omega_H+\frac{2A\omega_M k^2}{\mu_0 M_s^2}+\omega_M F\right)}. \tag{2}$$

In this expression, $F=P_k+\sin\delta^2[1-P_k(1+\cos\theta^2)]+\omega_M\frac{P_k(1-P_k)\sin\theta^2}{\omega_H+2A\omega_M k^2/\mu_0 M_s^2}$, $P_k=1-\frac{1-\exp(-kd)}{kd}$, $\omega_M=\gamma\mu_0 M_s$, and $\omega_H=\gamma\mu_0 H_{ani}$, where M_s is the saturation magnetization, θ is the angle between the wave vector k and the magnetization direction, H_{ani} is the magnetic anisotropy field, and d is the Fe film thickness. In $Fe/BaTiO_3$ with in-plane magnetization, $\delta=\pi/2$, $\gamma/2\pi=29$ GHz/T, and

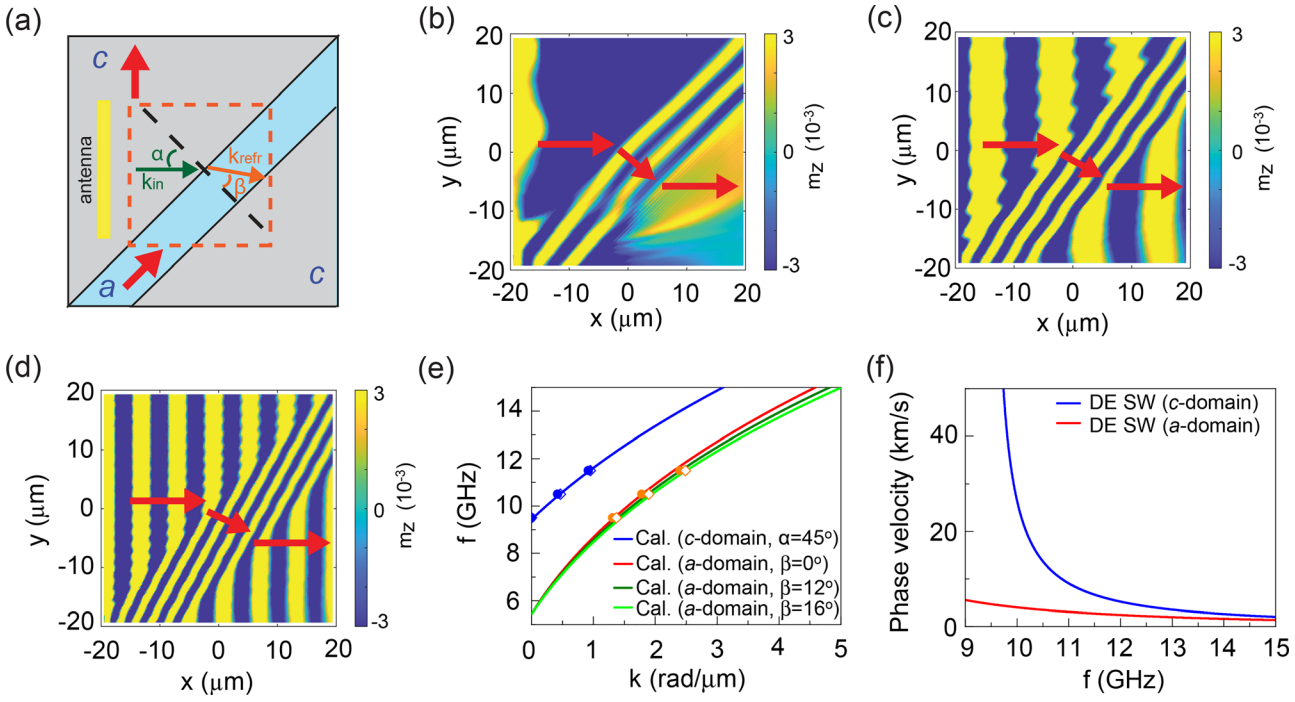

FIG. 2. (a) Schematic of the $c-a-c$ domain structure used in micromagnetic simulations. Red arrows depict the magnetization direction in the domains. (b)–(d) Simulated spatial maps of spin-wave transport at 9.5 GHz (b), 10.5 GHz (c), and 11.5 GHz (d). The displayed area corresponds to the dashed box shown in (a). Red arrows indicate the direction of spin-wave propagation. (e) Measured (solid symbols), simulated (empty symbols), and calculated (lines) spin-wave dispersion relations for the a and c domains. (f) Phase velocity of DE spin waves in the a and c domains as a function of frequency.

$H_{ani} = 2K_c/M_s$ for the c domain and $H_{ani} = 2K_a/M_s$ for the a domain. In our experiments, the incident angle α is fixed by the orientation of the microwave antenna and k_{in} can be calculated using Eq. (2). Knowing α and k_{in}, the refraction angle β and the wave vector in the a domain are then derived from Eqs. (1) and (2).

Figure 3(a) compares the calculated routing angle ($\gamma = \alpha - \beta$) to the experimental and simulation results for $\alpha = 45°$. Good agreement between the three data sets confirms the validity of Snell's law. At $\alpha = 45°$, the routing angle diminishes from about 45° to 20° when the frequency increases from 9.5 to 20 GHz. A smaller difference in phase velocity between the c and a domains at high frequency explains this effect [Fig. 2(f)]. Larger routing angles can be attained by increasing the angle of incidence, as demonstrated for $\alpha = 60°$ in Fig. 3(b). Together with the data for $\alpha = 30°$ [also shown in Fig. 3(b)], it is clear that the routing angle γ equals α (i.e., $\beta = 0°$) at the onset of spin-wave transport ($f \approx 9.5$ GHz) for all incident angles. Tuning of spin-wave routing by the angle of incidence at $f = 10.5$ GHz is depicted in Fig. 3(c). Finally, we illustrate how the routing angle changes as a function of magnetic anisotropy strength. The data depicted in Fig. 3(d) are calculated at 13.5 GHz for a varying anisotropy strength in the c domain, while keeping the anisotropy value of the a domain constant at $K_a = 15 \times 10^3$ J/m^3. In multiferroic heterostructures, the magnetic anisotropy strength can be tuned by interface strain engineering or the selection of ferromagnetic materials with different magnetostriction constants.

Our results open up perspectives for voltage-controlled routing of spin waves. The Fe/$BaTiO_3$ multiferroic heterostructure enables reversible control over the width of the a and c domains by the application of voltages across the ferroelectric substrate, as demonstrated in Refs. 29 and 30. For localized spin-wave transport in the c domain, an increase in the a-domain size would enhance the lateral shift of the spin-wave signal across the $c - a - c$ domain structure [see red arrows in Figs. 3(b)–3(d)], while a decrease in the a domain width would have the opposite effect. Combined with large and tunable routing angles in zero magnetic field, this sets the stage for all-electrical signal modulation in magnonic refractive-index gratings.

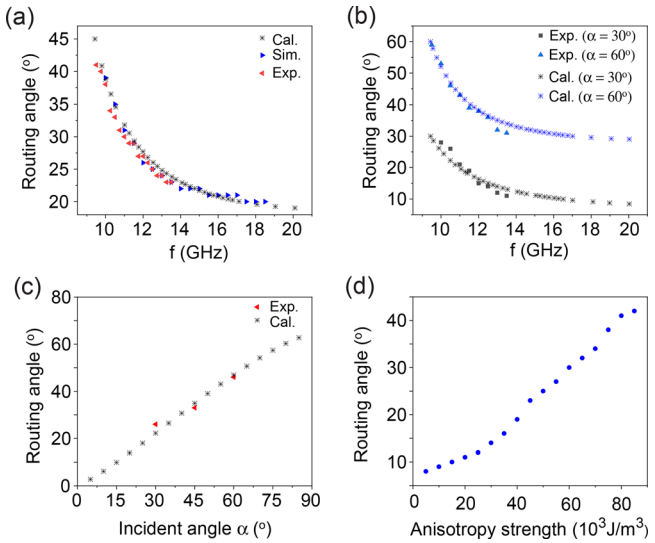

FIG. 3. (a) and (b) Dependence of the routing angle on spin-wave frequency for $\alpha = 45°$ (a), $\alpha = 30°$ (b), and $\alpha = 60°$ (b). (c) Routing angle as a function of the incident angle at a frequency of 10.5 GHz. (d) Dependence of the routing angle on the strength of magnetic anisotropy for $\alpha = 45°$ and $f = 13.5$ GHz. $K_a = 15 \times 10^3$ J/m^3 and K_c is varied.

This project has received funding from the European Union's Horizon 2020 research and innovation programme under the Marie Skłodowska-Curie grant agreement No. 861145. The work was supported by the Academy of Finland (Grant Nos. 317918 and 325480), JST CREST under Grant No. JPMJCR18J1, and JSPS KAKENHI under Grant No. 21H04614. Lithography was performed at the OtaNano—Micronova Nanofabrication Centre of Aalto University. Computational resources were provided by the Aalto Science-IT project.

AUTHOR DECLARATIONS

Conflict of Interest

The authors have no conflicts to disclose.

DATA AVAILABILITY

The data that support the findings of this study are available from the corresponding author upon reasonable request.

REFERENCES

[1]A. Khitun, M. Bao, and K. L. Wang, "Magnonic logic circuits," J. Phys. D. **43**, 264005 (2010).
[2]A. V. Chumak, V. I. Vasyuchka, A. A. Serga, and B. Hillebrands, "Magnon spintronics," Nat. Phys. **11**, 453–461 (2015).
[3]A. V. Chumak, A. A. Serga, and B. Hillebrands, "Magnonic crystals for data processing," J. Phys. D **50**, 244001 (2017).
[4]A. Mahmoud, F. Ciubotaru, F. Vanderveken, A. V. Chumak, S. Hamdioui, C. Adelmann, and S. Cotofana, "Introduction to spin wave computing," J. Appl. Phys. **128**, 161101 (2020).
[5]A. Barman, G. Gubbiotti, S. Ladak *et al.*, "The 2021 magnonics roadmap," J. Phys.: Condens. Matter **33**, 413001 (2021).
[6]A. V. Chumak, P. Kabos, M. Wu *et al.*, "Roadmap on spin-wave computing," arXiv:2111.00365 (2021).
[7]P. Clausen, K. Vogt, H. Schultheiss, S. Schäfer, B. Obry, G. Wolf, P. Pirro, B. Leven, and B. Hillebrands, "Mode conversion by symmetry breaking of propagating spin waves," Appl. Phys. Lett. **99**, 162505 (2011).
[8]K. Vogt, H. Schultheiss, S. Jain, J. E. Pearson, A. Hoffmann, S. D. Bader, and B. Hillebrands, "Spin waves turning a corner," Appl. Phys. Lett. **101**, 042410 (2012).
[9]X. Xing, Y. Yu, S. Li, and X. Huang, "How do spin waves pass through a bend?," Sci. Rep. **3**, 2958 (2013).
[10]X. Xing, W. Yin, and Z. Wang, "Excitation of antisymmetric modes and modulated propagation of spin waves in bent magnonic waveguides," J. Phys. D **48**, 215004 (2015).
[11]A. V. Sadovnikov, C. S. Davies, V. V. Kruglyak, D. V. Romanenko, S. V. Grishin, E. N. Beginin, Y. P. Sharaevskii, and S. A. Nikitov, "Spin wave propagation in a uniformly biased curved magnonic waveguide," Phys. Rev. B **96**, 060401 (2017).
[12]C. S. Davies, A. V. Sadovnikov, S. V. Grishin, Y. P. Sharaevsky, S. A. Nikitov, and V. V. Kruglyak, "Field-controlled phase-rectified magnonic multiplexer," IEEE Trans. Magn. **51**, 3401904 (2015).
[13]C. S. Davies and V. V. Kruglyak, "Graded-index magnonics," Low Temp. Phys. **41**, 760–766 (2015).
[14]P. Gruszecki and M. Krawczyk, "Spin-wave beam propagation in ferromagnetic thin films with graded refractive index: Mirage effect and prospective applications," Phys. Rev. B **97**, 094424 (2018).
[15]N. J. Whitehead, S. A. R. Horsley, T. G. Philbin, and V. V. Kruglyak, "A Luneburg lens for spin waves," Appl. Phys. Lett. **113**, 212404 (2018).

[16]N. J. Whitehead, S. A. R. Horsley, T. G. Philbin, and V. V. Kruglyak, "Graded index lenses for spin wave steering," Phys. Rev. B **100**, 094404 (2019).
[17]S. Mieszczak, O. Busel, P. Gruszecki, A. N. Kuchko, J. W. Kłos, and M. Krawczyk, "Anomalous refraction of spin waves as a way to guide signals in curved magnonic multimode waveguides," Phys. Rev. Appl. **13**, 054038 (2020).
[18]M. Vogel, P. Pirro, B. Hillebrands, and G. von Freymann, "Optical elements for anisotropic spin-wave propagation," Appl. Phys. Lett. **116**, 262404 (2020).
[19]O. Dzyapko, I. V. Borisenko, V. E. Demidov, W. Pernice, and S. O. Demokritov, "Reconfigurable heat-induced spin wave lenses," Appl. Phys. Lett. **109**, 232407 (2016).
[20]M. Vogel, R. Aßmann, P. Pirro, A. V. Chumak, B. Hillebrands, and G. von Freymann, "Control of spin-wave propagation using magnetisation gradients," Sci. Rep. **8**, 11099 (2018).
[21]J. Stigloher, M. Decker, H. S. Körner, K. Tanabe, T. Moriyama, T. Taniguchi, H. Hata, M. Madami, G. Gubbiotti, K. Kobayashi, T. Ono, and C. H. Back, "Snell's law for spin waves," Phys. Rev. Lett. **117**, 037204 (2016).
[22]J.-N. Toedt, M. Mundkowski, D. Heitmann, S. Mendach, and W. Hansen, "Design and construction of a spin-wave lens," Sci. Rep. **6**, 33169 (2016).
[23]W. Yu, J. Lan, R. Wu, and J. Xiao, "Magnetic Snell's law and spin-wave fiber with Dzyaloshinskii-Moriya interaction," Phys. Rev. B **94**, 140410 (2016).
[24]Á. Papp and G. Csaba, "Lens design for computing with anisotropic spin waves," IEEE Magn. Lett. **9**, 3706405 (2018).
[25]J. Mulkers, B. Van Waeyenberge, and M. V. Milošević, "Tunable Snell's law for spin waves in heterochiral magnetic films," Phys. Rev. B **97**, 104422 (2018).
[26]T. Hioki, R. Tsuboi, T. H. Johansen, Y. Hashimoto, and E. Saitoh, "Snell's law for spin waves at a 90° magnetic domain wall," Appl. Phys. Lett. **116**, 112402 (2020).
[27]K. J. A. Franke, T. H. E. Lahtinen, and S. van Dijken, "Field tuning of ferromagnetic domain walls on elastically coupled ferroelectric domain boundaries," Phys. Rev. B **85**, 094423 (2012).
[28]T. H. E. Lahtinen, Y. Shirahata, L. Yao, K. J. A. Franke, G. Venkataiah, T. Taniyama, and S. van Dijken, "Alternating domains with uniaxial and biaxial magnetic anisotropy in epitaxial Fe films on $BaTiO_3$," Appl. Phys. Lett. **101**, 262405 (2012).
[29]K. J. A. Franke, B. Van de Wiele, Y. Shirahata, S. J. Hämäläinen, T. Taniyama, and S. van Dijken, "Reversible electric-field-driven magnetic domain-wall motion," Phys. Rev. X **5**, 011010 (2015).
[30]H. Qin, R. Dreyer, G. Woltersdorf, T. Taniyama, and S. van Dijken, "Electric-field control of propagating spin waves by ferroelectric domain-wall motion in a multiferroic heterostructure," Adv. Mater. **33**, 2100646 (2021).
[31]H. Qin, R. B. Holländer, L. Flajsman, F. Hermann, R. Dreyer, G. Woltersdorf, and S. van Dijken, "Nanoscale magnonic Fabry-Pérot resonator for low-loss spin-wave manipulation," Nat. Commun. **12**, 2293 (2021).
[32]S. J. Hämäläinen, M. Madami, H. Qin, G. Gubbiotti, and S. van Dijken, "Control of spin-wave transmission by a programmable domain wall," Nat. Commun. **9**, 4853 (2018).
[33]A. Vansteenkiste, J. Leliaert, M. Dvornik, M. Helsen, F. Garcia-Sanchez, and B. Van Waeyenberge, "The design and verification of MuMax3," AIP Adv. **4**, 107133 (2014).
[34]S.-K. Kim, "Micromagnetic computer simulations of spin waves in nanometre-scale patterned magnetic elements," J. Phys. D **43**, 264004 (2010).
[35]B. A. Kalinikos and A. N. Slavin, "Theory of dipole-exchange spin wave spectrum for ferromagnetic films with mixed exchange boundary conditions," J. Phys. C **19**, 7013 (1986).